



Contents lists available at ScienceDirect

## International Communications in Heat and Mass Transfer

journal homepage: [www.elsevier.com/locate/ichmt](http://www.elsevier.com/locate/ichmt)

# Topology optimization of heat source distribution for volume-to-point heat conduction

Zhi-Ke Liu, Han-Ling Li, Bing-Yang Cao\*

Key Laboratory for Thermal Science and Power Engineering of Ministry of Education, Department of Engineering Mechanics, Tsinghua University, Beijing 100084, China

## ARTICLE INFO

### Keywords:

Topology optimization  
Heat source distribution  
Volume-to-point heat conduction  
Equivalent distance function

## ABSTRACT

Optimizing the heat source distribution is an effective strategy to enhance the heat dissipation in electronic devices. In this paper, a topology optimization (TO) scheme with a penalty factor between 0 and 1 is developed to solve the volume-to-point heat source distribution. The topology-optimized heat source always lies around the heat sink with continuous design, and the isotherms show semicircular arcs with the semicircle center located at the heat sink. Compared with other optimization methods, the current TO method obtains better designs approximate to the theoretical optimal solution with higher cooling performance and lower computational cost. Moreover, an equivalent distance function reflecting the distance between the heat source and the heat sink is introduced to evaluate the performance of different heat source distributions. Topology-optimized designs and mathematical analyses show that reducing the equivalent distance between the heat source and the heat sink is an effective way to enhance heat transport. This work extends the application of the TO method and deepens the understanding of the optimization of heat source distribution.

## 1. Introduction

With the rapid development of modern science and technology, the scale of electronic devices becomes smaller and smaller, and the power density increases greatly [1]. For example, the power density in insulated-gate bipolar transistor (IGBT) chips has increased from 35 kW/cm<sup>2</sup> to 250 kW/cm<sup>2</sup> over the past three decades [2]. In addition, the heat generation in chip architectures can be highly non-uniform across the die surface, and the power density in localized functional areas is five to ten times higher than the die average, forming 'hot spots' in transistors [3]. Therefore, heat dissipation has become a key issue affecting the development of microelectronics technology [4,5]. High temperature can hinder the normal operation of electronic devices. It has been shown that more than 50% of electronic challenges are caused by the failure of thermal management [6,7], and that the reliability of electronic components will be halved for each 10 °C rise in their junction temperature [8]. Electronic devices and systems require uniform temperature field as well since non-uniform temperature field will affect the consistency of electronic equipment, resulting in a significant decline in performance and the lifetime of equipment [9]. In order to reduce the working temperature and improve the temperature uniformity of electronic devices, it is highly desired to optimize the heat dissipation of electronic

devices [10,11].

A typical strategy to enhance heat transport is to insert a certain amount of high thermal conductivity materials, such as carbon fiber [12] or diamond [13], into heat dissipation domain, and design its distribution, which can be abstracted as volume-to-point (VP) heat conduction [14]. As shown in Fig. 1(a), constant heat source intensity is generated in the square system as heat source, and heat flows out through a small heat sink with uniform temperature at the boundary, while other boundaries are adiabatic. The design objective is to find an optimal distribution of high thermal conductivity materials, constructing high thermal conductivity channels which can minimize the temperature (average or maximum temperature) of the whole system. Several optimization methods have been developed to study the VP problem, including constructive theory [14], bionic optimization (BO) [15], topology optimization (TO) [16–18], simulated annealing (SA), genetic algorithm [19], thermal conductivity discretization algorithm [20], conductivity spreading approach [21], and heat flow paths identification [22]. Among these optimization methods, TO has recently attracted great attention owing to its advantages in the exhaustive exploration of the design space [23], large degrees of freedom (DOF) of design [24], and improving the efficiency of heat transfer [25]. TO is the mathematical science of distributing material in an optimum manner for

\* Corresponding author.

E-mail address: [caoby@tsinghua.edu.cn](mailto:caoby@tsinghua.edu.cn) (B.-Y. Cao).

<https://doi.org/10.1016/j.icheatmasstransfer.2022.106304>

Available online 13 August 2022

0735-1933/© 2022 Elsevier Ltd. All rights reserved.

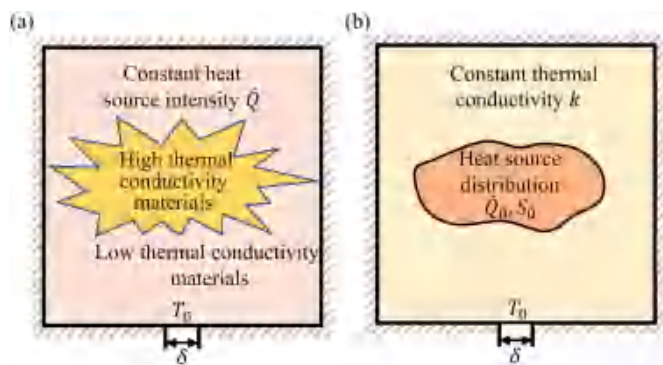


Fig. 1. Schematic diagram of the geometries and boundary conditions for the optimization of heat dissipation. (a) The classical VP with filling high thermal conductivity materials; (b) the VP heat source distribution.

predefined objectives and constraints [26]. TO for VP problem obtains high thermal conductivity material distributions similar to a natural tree with full penetration of inserted material into the internal domain [27], and its design results are better than those of other methods [28]. The experimental results verify the usefulness of the tree-like heat conductive structures [29]. In recent years, based on phonon Boltzmann transport equation, TO for ballistic-diffusive heat conduction at micro- and nano- scale has been developed [30]. However, due to spatial constraints and manufacturing costs, the application of filling high thermal conductivity materials is severely limited in actual problems.

Another common scheme to enhance heat transport is the optimization of heat source distribution, that is, optimizing the location of heat sources in the allowable space, so as to reduce the average or maximum temperature of the system. Without adding additional high thermal conductivity materials, this scheme is widely used in practice, such as: (1) optimum thermal design of chip placement of multi-chip module (MCM) in electronic packaging [31]; (2) placement of heat generating semiconductor logic blocks on integrated circuit chips [32,33]; (3) finding optimal location of discrete heat sources inside a cavity with convection [34,35]. Take the thermal design of MCM as an example. MCM contains multiple chips, and each chip is regarded as a heat source. The purpose is to design the heat source distribution for reducing temperature and improving temperature uniformity. It can be abstracted as a VP heat source distribution by referring to the classical VP problem filled with high thermal conductivity materials [36]. As shown in Fig. 1 (b), the square system represents MCM, in which a material with constant thermal conductivity is filled. In the case of a prescribed volume constraint of heat sources, heat is dissipated to a small patch of heat sink with uniform temperature and other boundaries are adiabatic. The design objective is to adjust the distribution of heat sources to reduce the temperature (average or maximum temperature) of the whole system. Several optimization methods have been adopted to design the heat source distribution, including BO [36,37], SA [38] and convex optimization (CO) [39]. Compared to random distribution of heat sources, the above methods can reduce the system temperature and improve the temperature uniformity, but there are still some limits: (1) The general principle of optimization is unclear, as the optimized heat source distribution varies with the optimization methods; (2) The optimizations of different MCMs are hard to conduct considering the relatively high computational costs; (3) The optimized heat source blocks are generally discrete, which hinders the performance of the optimization. These are closely enslaved to the optimization methods themselves.

TO has not been applied to the optimization of heat source distribution thus far although it has advantages of larger number of DOF and less computational time. Since the design variable changes from the distribution of high conductivity materials to the distribution of heat sources, the way to choose the relevant optimization parameters in TO changes. In the present work, TO for VP heat source distribution is

developed. A solid isotropic material with penalization (SIMP) method whose penalty factor is between 0 and 1 is employed to interpolate the heat source intensity, and the gray transition region is alleviated by the projection technique. The topology-optimized heat source always lies around the heat sink with continuous designs, which better approximates the theoretical optimal solution. At the same time, the performance and computational cost of TO are better than those of the existing optimization methods. Furthermore, it is suitable for more optimization scenarios, though complex geometry, different material interfaces, and different ambient conditions need to be carefully considered.

## 2. Methodology

### 2.1. Volume-to-point system

As shown in Fig. 1(b), the side length of the system is chosen as  $a$ . The thermal conductivity of the material is  $k$ . The width of the heat sink is  $\delta$ , with uniform temperature value  $T_0$ . Heat sources are distributed in the system with constant intensity ( $\dot{Q}_0$ ). The region where heat sources are distributed is defined as the heat source domain, and its area is  $S_0$ , and the ratio of  $S_0$  to the area of the whole system ( $S$ ) is the volume constraint of heat sources ( $\phi$ ), that is  $S_0 = \phi S$ . The remaining domain is defined as the non-heat-source domain. Compared with the optimization of high thermal conductivity materials, the heat source domain is more noteworthy in the optimization of heat source distribution, which is conducive to reducing the maximum temperature and improving the temperature uniformity. Consequently, the average temperature of the domain weighted by the heat source intensity [40,41].  $T_{\text{avg}} = \int_S \dot{Q} T dS / \int_S \dot{Q} dS$  is used as the objective function for optimization, in which  $\dot{Q}$  is the intensity of heat sources at any location in  $S$ . In the heat source domain ( $S_0$ ),  $\dot{Q}$  is equal to the prescribed value  $\dot{Q}_0$ , thus in the whole square system,  $T_{\text{avg}}$  can be written as

$$T_{\text{avg}} = \frac{1}{S_0} \int_{S_0} T dS. \quad (1)$$

In this way,  $T_{\text{avg}}$  can be understood as the average temperature of the heat source domain. In practice, the temperature control in the heat source domain is generally more important than that in other domains. According to the actual demand, the arithmetic average temperature, the maximum temperature or the temperature gradient can also be selected as the objective functions. In practical application, the heating situation of heat source is complicated. Physics-based analytical models have been reported with significant computational efficiency [42]. According to the formation mechanism of heat source, different heat source models can be appropriately simplified and applied to optimization [43]. Ning and Liang evaluate the prediction accuracy, computational efficiency, and experimental complexity of several analytical models, showing the superiority of the model they developed. [44]. In this work, the average temperature of the heat source domain is taken as an example for discussion.

### 2.2. Topology optimization

TO is originally a discrete 0–1 design and naturally has severe numerical instabilities [45]. The basic principle to implement TO is to replace the original discrete optimization with the continuous one where the design variable varies continuously between 0 and 1. In this regard, SIMP method [46,47] is a commonly used technique. Its key idea is to set the properties to be optimized as a power function of design variable, so as to transform the properties into continuous. A SIMP method of interpolating heat source intensity is used to realize TO of heat source distribution. Construct a heat generation function, and the intensity of heat sources at any location in the system can be written as

$$\dot{Q}(\rho) = \dot{Q}_0 \rho^p, \quad (2)$$

where  $\rho$  is the design variable field that varies continuously in the interval  $[0,1]$ , and  $p$  is the penalty factor. The function of  $p$  is to penalize intermediate design variables to drive  $\rho$  towards the bounds of 0 and 1, so that the clear distribution of void ( $\rho = 0$ , indicating no heat source) and solid ( $\rho = 1$ , indicating heat generation with  $\dot{Q}_0$ ) is obtained, and the continuous solution tends to the discrete one. In existing literature using the SIMP model,  $p > 1$  is adopted, and  $p = 3$  is an often-used value [48]. However, for TO of interpolating heat source intensity,  $p$  should be set between 0 and 1. To illustrate the selection principle of  $p$ , the concepts of “costs”, “earnings” and “net earnings” are introduced. “Costs” is defined as the amount of the design variable ( $\rho$ ), “earnings” is defined as the amount of heat source intensity obtained from consuming costs ( $\rho^p$ ), and “net earnings” is defined as the difference between earnings and costs ( $\rho^p - \rho$ ). “Earnings” and “net earnings” varying with “costs” are shown in Fig. 2 (a) and (b), respectively. For the linear interpolation of  $p = 1$ , the net earnings are always 0, indicating that different values of the design variable have the same interpolation effect. For the nonlinear interpolation of  $p \neq 1$ , the net earnings are 0 at the bounds of 0 and 1, but different in the interval (0,1). If  $p > 1$ , the net earnings of intermediate design variables are lower than those of the bounds of 0 and 1, which is opposite if  $p < 1$ . Taking  $\rho = 0.5$  as an example, in Fig. 2(b), the order of net earnings of different curves from high to low are  $p = 0.4, p = 0.8, p = 1, p = 3, p = 5$ . In the SIMP method, the penalty factor cannot equal 1, so that the net earnings of intermediate design variables are different from those of the bounds. In this case, under the volume constraint of costs, intermediate design variables are “not cost-effective”, which are automatically punished. When the thermal conductivity is interpolated,  $p > 1$  is taken to make the interpolation curves concave, and the net earnings of intermediate design variables is lower than those of the bounds, so as to penalize intermediate design variables [49,50]. The higher the interpolation net earnings are, the more conducive it is to enhance the heat dissipation. However, in the optimization of heat source distribution, heat source intensity is interpolated. If  $p < 1$ , the interpolation curves are convex function, and the net earnings are the lowest at the bounds of 0 and 1. The lower the net earnings of interpolation are, the lower the temperature rise. In this case, intermediate design variables will hinder the reduction of the objective function, so that intermediate design variables are penalized as much as possible. The specific value of  $p$  will be determined based on the calculation results in Section 3.1.

An inherent problem of using the continuous design variable is the gray transition regions between solid and void parts, which means that the solid/void interfaces in the optimized solutions are not discrete 0/1 transitions but smeared out. This can be alleviated by projection methods, and here we use the threshold Heaviside function projection [51,52].

$$\rho_p = \frac{\tanh(\sigma\eta) + \tanh(\sigma(\rho - \eta))}{\tanh(\sigma\eta) + \tanh(\sigma(1 - \eta))} \quad (3)$$

where  $\sigma, \eta, \rho_p$  denote the projection steepness, the projection threshold,

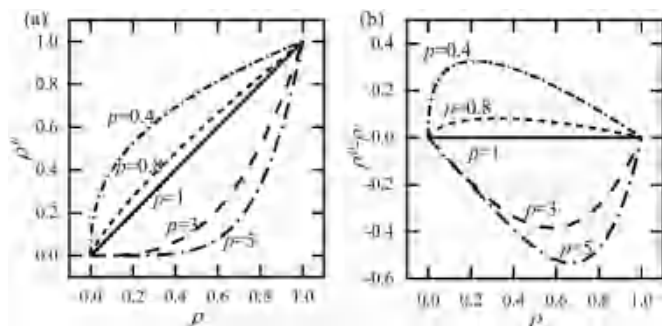


Fig. 2. Schematic of the SIMP method. (a) Earnings - Costs; (b) Net earnings - Costs.

and the projected design variable, respectively. It is important to note that  $\rho_p$  is the physically meaningful material density used in Eq. (2), and for the following figures illustrating the topology-optimized heat sources, the distributions of  $\rho_p$  are shown.

The mathematic model of the heat source distribution by TO is shown as follows.

$$\begin{aligned} \min_{0 \leq \rho \leq 1} & : g = T_{\text{avg}}, \\ \text{s.t.} & : \nabla \cdot (k \nabla T) + \dot{Q} = 0 \\ & \dot{Q}(\rho) = \dot{Q}_0 \cdot \rho_p^p \\ & \rho_p = \frac{\tanh(\sigma\eta) + \tanh(\sigma(\rho - \eta))}{\tanh(\sigma\eta) + \tanh(\sigma(1 - \eta))} \\ & \int \rho_p \, dS \geq \phi S. \end{aligned} \quad (4)$$

The solution of TO of heat source distribution involves the following procedures: (1) Discretization and initialization. The initial design is  $\rho_{\text{init}} = \phi$ , that is, the uniform distribution of heat sources in the system. (2) System reanalysis. For a given design variable distribution, heat source intensity is interpolated using Eq. (2). The finite element method is employed to numerically solve the heat diffusion equation, and the temperature field is obtained. (3) Sensitivity analysis. In order to apply gradient-based optimization algorithms to TO, the adjoint method [53] is adopted to calculate the sensitivities, which refers to the gradients of the objective function and constraint functions to the design variables. (4) Projection. The design field is projected by Eq. (3). (5) Optimization. The well-known method of moving asymptotes [54] is employed since it is especially compatible with TO. (6) Convergence judgment. Repeating steps (2)–(5) unless the convergence criterion is satisfied. The heat diffusion equation in Eqs. (4) are solved by the Heat Transfer in Solids (ht) module of COMSOL Multiphysics.

### 3. Results and discussion

In this work, the VP heat conduction parameters are  $a = 0.1 \text{ m}$ ,  $\delta = 0.001 \text{ m}$ ,  $T_0 = 298 \text{ K}$ ,  $k = 1 \text{ W/(m} \cdot \text{K)}$ ,  $\dot{Q}_0 = 10000 \text{ W/m}^2$ ,  $\eta = 0.5$ . For the sake of comparison, the parameters and results are non-dimensionalized as  $X = x/a$ ,  $Y = y/a$ ,  $\delta^* = \delta/a$ ,  $T^* = (T - T_0) / (\dot{Q}_0 a^2 / k)$  [36]. In the finite element method, the square mesh number is  $n \times n$ . The stopping criterion is  $\|\rho_p^i - \rho_p^{i-1}\|_{\infty} \leq 0.001$  or the iteration number denoted as superscript  $i$  reaches a maximum value of 60. When this condition is satisfied, the design variables and objective values are stable.

In order to evaluate the performance of the solution, three dimensionless metrics are introduced. The first one is the non-dimensional average temperature of the domain weighted by the heat source intensity, which is defined as

$$T_{\text{avg}}^* = \frac{\frac{1}{\dot{Q}_0 n^2} \sum_{j=1}^{n^2} T_j \dot{Q}_j - T_0}{\dot{Q}_0 a^2 / k}, \quad (5)$$

where  $T_j$  and  $\dot{Q}_j$  denote the temperature and the heat source intensity of each mesh, respectively.  $T_{\text{avg}}^*$  represents the objective value. The second is the non-dimensional maximum temperature defined as

$$T_{\text{max}}^* = \frac{T_{\text{max}} - T_0}{\dot{Q}_0 a^2 / k}, \quad (6)$$

where  $T_{\text{max}}$  is the maximum temperature of the whole system. The third is the non-dimensional standard deviation, that is

$$\sigma_T^* = \frac{1}{\dot{Q}_0 a^2 / k} \sqrt{\frac{1}{n^2} \sum_{j=1}^{n^2} (T_j - T_{S,avg})^2}, \quad (7)$$

where  $T_{S,avg} = \sum_{j=1}^{n^2} T_j / n^2$  is average temperature of the whole system. A smaller  $\sigma_T^*$  represents a more uniform temperature field.

### 3.1. Topology-optimized distribution

At first, the penalty factor ( $p$ ) should be determined in order to design the heat source distribution with the given boundary conditions. Setting  $\phi = 0.1$ ,  $n = 200$ ,  $\sigma = 10$ , the topology-optimized designs and objective values ( $T_{avg}$ ) varying with the penalty factor are shown in Fig. 3. The gray-scale maps show the distributions of  $\rho$ , in which the black and white regions represent the heat source domain ( $\rho = 1$ ) and the non-heat-source domain ( $\rho = 0$ ), respectively. The deeper the color is, the closer the value of  $\rho$  is to 1. The boundary between the heat source domain and the non-heat-source domain seems unclear when  $p = 0.1$ , while the heat source distribution is roughly similar under the other values of  $p$ . The objective value decreases from 342.88 K to 311.35 K as  $p$  increases, indicating that a smaller  $p$  results in a lower objective value. However, if  $p$  continues to increase, the optimization process will become unstable because  $p$  is too close to 1. After careful comparisons, it is determined that  $p = 0.8$  is a reasonable value.

Then, it is necessary to verify the feasibility of the current TO method and test the mesh independence. Topology-optimized designs and objective values varying with the mesh number ( $n$ ) and the projection steepness ( $\sigma$ ) are shown in Fig. 4. In general, the outlines of the heat source domain are approximately semi-circular, but are different in detail. For the results of  $\sigma = 0$ , there are a large area of gray transition regions at different mesh sizes, and the boundaries of the heat source distribution look unclear, since the calculation quickly reaches the convergence criterion and the optimization stops. When  $\sigma$  reaches to 5, the area of gray transition regions decreases greatly, and the designs at different  $n$  are basically the same. When  $\sigma = 10$ , the boundary between the heat source domain and the non-heat-source domain becomes clearer, exhibiting a strong mesh-dependence. The design is sawtooth and there is still gray transition region at  $n = 100$ , while it becomes clear and regular at  $n = 200$  and  $n = 400$ . If  $\sigma$  continues to increase, the projection effect is too strong, affecting the stability of the optimization process. The objective value decreases as  $\sigma$  increases, and for the 9 examples in Fig. 4, the objective value corresponding to  $n = 200$ ,  $\sigma = 10$  is the smallest, i.e.  $T_{avg} = 311.35$  K. In our work,  $n = 200$ ,  $\sigma = 10$  are recommended, since it has lower objective value, stronger mesh-dependence, better numerical stability, clearer domain boundary, and higher calculation efficiency.

The temperature field obtained by TO corresponding to  $p = 0.8$ ,  $n = 200$ ,  $\sigma = 10$  is given in Fig. 5. The region surrounded by the black curve denotes the heat source domain, and the semicircle center is located at the heat sink. In addition, the isotherms also look like semi-circular arcs,

similar to the profile of the heat source distribution. The underlying mechanisms for the above distribution and isotherms obtained by TO point to minimization of the distance between the heat source and the heat sink, which will be discussed in detail below.

The reference [36] proved that the optimal scheme is that the heat source is located on the boundaries where heat can flow out. In practice, the heat source occupies a certain area and cannot be distributed in a line segment, but it is still the best design to reduce the distance between the heat source and the heat sink. Mathematical analyses can be further applied to predict the optimal heat source distribution. According to the heat diffusion equation with heat generation under steady-state and constant thermal conductivity, it obtains

$$k \int_S [(\nabla T)^2] dS = \int_S \dot{Q} T dS - \dot{Q}_0 S_0 T_0, \quad (8)$$

where  $\int_S \dot{Q} T dS = T_{avg} \cdot \dot{Q}_0 S_0$  and  $\dot{Q}_0 S_0 T_0$  is fixed value. Therefore, the problem of finding a minimum for objective function ( $T_{avg}$ ) can be transformed into finding a minimum for  $k \int_S [(\nabla T)^2] dS$ . Consider the temperature field of the heat source domain in polar coordinates. As shown in Fig. 6, the profile of heat source is approximately annular, and its inner radius ( $r_0$ ) equals half of the heat sink width ( $\delta$ ) with a boundary at  $T_0$ , while the outer radius ( $r(\varphi)$ ) is a function related to the polar angle ( $\varphi$ ) with an adiabatic boundary. In a radial system, the heat diffusion equation can be written as

$$\frac{1}{r} \frac{d}{dr} \left( r \frac{dT}{dr} \right) + \frac{\dot{Q}}{k} = 0. \quad (9)$$

Substituting boundary condition  $\frac{dT}{dr}|_{r=r(\varphi)} = 0$  into Eq. (9), we have

$$k \int_S [(\nabla T)^2] dS \approx \frac{\dot{Q}^2}{4k} \int_0^\pi \left[ \frac{r^4(\varphi)}{4} - r^4(\varphi) + r^4(\varphi) \ln \frac{r(\varphi)}{r_0} + r^2(\varphi) r_0^2 - \frac{r_0^4}{4} \right] d\varphi, \quad (10)$$

where  $\ln \frac{r(\varphi)}{r_0}$  can be regarded as a constant if  $r(\varphi)$  changes little.  $r^2(\varphi) r_0^2 - \frac{r_0^4}{4}$  can be ignored since  $r_0$  is much smaller than  $r(\varphi)$ . It obtains

$$k \int_S [(\nabla T)^2] dS \approx \frac{\dot{Q}^2}{4k} \int_0^\pi [b r^4(\varphi)] d\varphi, \quad (11)$$

where  $b$  is a constant. The constraint function is that the area of the heat source domain is fixed

$$\int_0^\pi d\varphi \int_{r_0}^{r(\varphi)} r(\varphi) r dr = S_0. \quad (12)$$

The condition of extreme value of Eq. (11) is obtained by the variational method

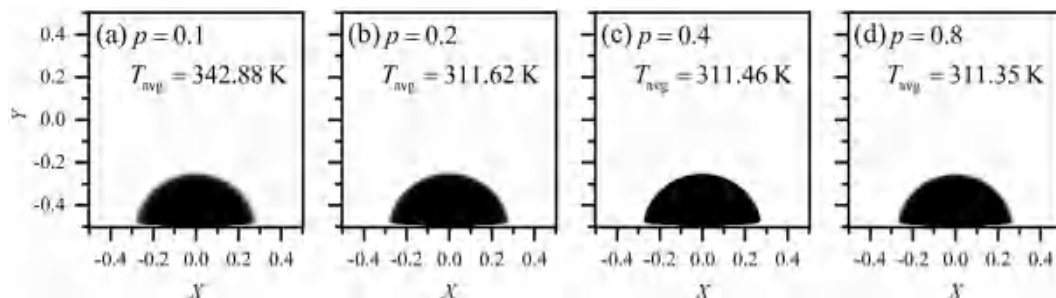


Fig. 3. Topology-optimized designs and objective values ( $T_{avg}$ ) varying with the penalty factor ( $p$ ). The black and white regions in the gray-scale map represent the heat source domain and the non-heat-source domain, respectively.

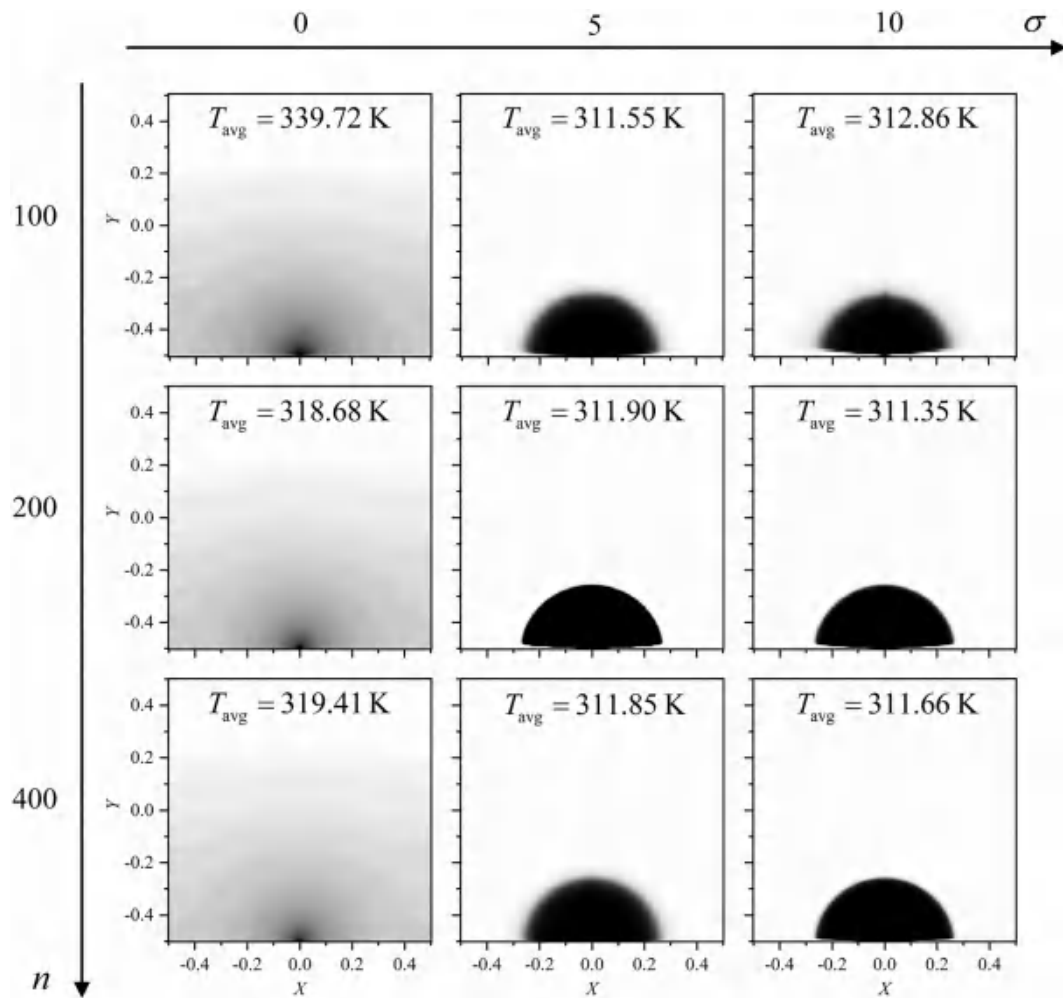


Fig. 4. Topology-optimized designs and objective values varying with the mesh number ( $n$ ) and the projection steepness ( $\sigma$ ) at  $p = 0.8$ .

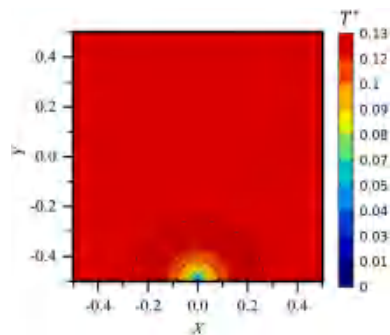


Fig. 5. Temperature field obtained by TO at  $\phi = 0.1$ .

$$r(\varphi) = \sqrt{\frac{2S_0}{\pi}}, \tag{13}$$

that is,  $r(\varphi)$  is a fixed radius of a semicircle corresponding to area  $S_0$ . Thus, it is theoretically proven that the profile of the optimized heat source domain is approximately semicircular.

It is also noted that the integral on the right side of Eq. (11) is directly related to the objective function, so the equivalent distance function can be defined as

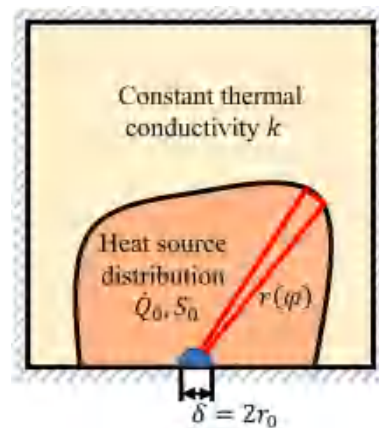


Fig. 6. Schematic diagram of the heat source distribution assumption.

$$D_p = \int_S r^2 dS = \int_0^\pi \left[ \frac{1}{4} r^4(\varphi) \right] d\varphi, \quad (14)$$

and

$$k \int_S [(\nabla T)^2] dS = \frac{b\dot{Q}^2}{k} D_p. \quad (15)$$

Here,  $b, \dot{Q}, k$  are constants, so  $D_p$  can be used to characterize the objective function. Given different heat source distributions, the temperature performance of different heat source distributions can be compared by calculating  $D_p$  without solving the heat diffusion equation. In this way, the calculation of the temperature field is simplified to the calculation of the geometric domain, which greatly facilitates the judgment of the optimization performance of the VP heat source distribution. In fact,  $D_p$  represents the integral of the square of the distance from each point in the domain to a given point. Meanwhile, the heat sink can be regarded as a point approximately in the VP heat source distribution.  $D_p$  of the heat source domain to the heat sink represents the distance between the heat source and the heat sink, so it can be used to measure the performance of heat source distributions.

In order to verify the above discussion, a rectangular non-design area where heat source cannot be distributed is set around the heat sink, as shown in Fig. 7(a). The geometric parameters of the rectangular area are  $c = 0.04$  m and  $d = 0.02$  m. With other parameters unchanged, TO is conducted and the results are shown in Fig. 7(b). The topology-optimized heat source is adjacent to the rectangular non-design area. Meanwhile, the outer edge of the heat source and the isotherms are still approximately semi-circular arc. Since the non-design area is not allowed to distribute heat source, TO places the heat source close to the edges of the rectangular area to reduce the distance between the heat source and the heat sink.

### 3.2. Comparison of TO and other optimization methods

In this section, the designs of TO are compared with those of BO, SA, and CO to analyze the performance of different optimization methods.  $\phi = 0.2$  is used so that the physical settings are consistent with those in the references [36, 38, 39]. In the three methods of BO, SA, and CO, the basic unit of heat sources is selected as 20 small squares with side length 0.01 m subject to the computational costs. The distributions are obtained from the above references, but the temperature field is recalculated to facilitate the comparison. For fairly performance comparisons, 20 small squares are rearranged referring to the distribution given by TO, and the new design is named "TO\*". The designs and temperature fields obtained by different optimization methods are plotted in Fig. 11, in which the small squares (BO, SA, CO, and TO\*) or black curve (TO) are the heat source domain. As expected, the design obtained by TO looks like a semi-circular distribution around the heat sink. The profiles

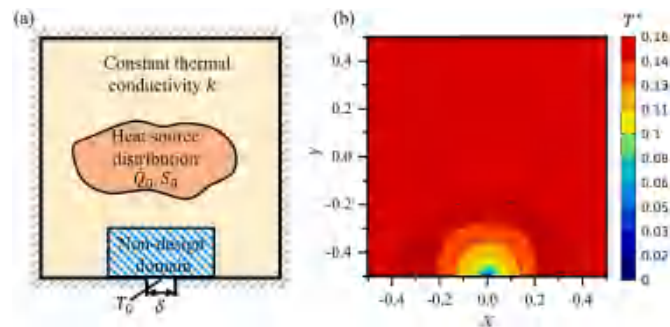


Fig. 7. TO with rectangular non-design area. (a) Schematic diagram of the geometries and boundary conditions; (b) topology-optimized design and temperature field.

of the squares optimized by other methods are also roughly semi-circular, but there are gaps (SA, CO) or dislocations (BO, SA) between the squares. In other words, these heat sources are not as close to the heat sink as possible with discrete and irregular distributions. In contrast, there is no gaps or dislocations between heat sources in TO\*. As a consequence, the designs of TO and TO\* are not only closer to the theoretical optimal solution, but also avoid the disadvantages of discrete distribution in other methods. Besides, the high temperature region ( $0.28 < T^* < 0.3$ ) of the temperature field obtained by TO and TO\* in Fig. 8 is smaller than the others, indicating a lower average temperature.

In order to quantitatively compare the results of each method,  $T_{avg}^*$ ,  $T_{max}^*$ ,  $\sigma_T^*$ , and  $D_p$  are listed in Table 1.  $T_{avg}^*$  of TO reaches 0.2633, which is reduced by more than 1.5% compared to other methods.  $T_{max}^*$  of TO, which is 0.2820, decreases compared with other methods, especially 5% lower than CO.  $\sigma_T^*$  of TO gets 0.01251, which is slightly reduced compared to BO, while it is 7.4% and 8.8% lower than SA and CO, respectively. If compared with TO\* which is not continuous, TO\* still occupies advantages in terms of the above metrics though slightly inferior to TO. For  $D_p$ , the value of TO is  $1.30 \times 10^{-6} m^4$ , slightly lower than that of BO, and significantly lower than those of SA and CO, with decreases of 16% and 21%, respectively. The variation trend of  $D_p$  with the optimization method is consistent with those of the temperature metrics, indicating that  $D_p$  can quickly and accurately evaluate the heat transport, so that the performance of different heat source distributions can be compared without calculating the temperature field. The heat source distributions in Fig. 8 have a similar tendency, namely BO is the closest to TO and TO\*, followed by SA and CO. Compared to the other three methods, TO effectively reduces the average temperature and the maximum temperature, and improves the temperature uniformity. TO is the best of the four methods in optimization performance which can approximate the theoretical optimal solution better.

In the evaluation of the optimization method, the computational costs should also be considered. In this respect, TO has two advantages. First, the computational cost of TO is independent of the number of heat sources in the system. If the edge length of small square heat sources optimized by other methods is infinitely small, the designs obtained by TO will be approximated. Therefore, TO can approximate the theoretical optimal solution better. Second, the computational cost of TO has little relation with the volume of heat sources ( $\phi$ ). That the design variable field ( $\rho$ ) of each mesh in TO is 0 or 1 does not directly affect the computational cost of TO. Increasing the number of heat sources or reducing the area of a single heat source can increase the computational time of the other three methods, but cannot change the efficiency and performance of TO. The total number of temperature field calculations of different methods are illustrated in Fig. 9, which in some extent reflects the computational costs. Reference [38] notes that the total number of temperature field calculations of SA and BO is proportional to the number of heat sources. For example, when the volume of heat sources is 0.2, the numbers are 1760 and 420 for SA and BO respectively, significantly higher than CO and TO. SA has the largest total number of temperature field calculations among the four methods, because annealing steps are nested in each cycle. For CO, the temperature field is calculated only twice [39]. However, due to the characteristics of CO itself, it is necessary to set the guaranteed minimum inter-source spacing. Consequently, the number of grid cells for placing the heat sources cannot be too small, which significantly affects the efficiency and performance of optimization. For TO, the computational cost mainly depends on the mesh number. In this work, the mesh number is  $200 \times 200$ , and the upper limit of the total number of temperature field calculations is set to 60, which can obtain reliable results.

### 3.3. Effects of heat source volume and heat sink width

MCMs may have different numbers of heat sources and different sizes of heat sinks, which will affect the optimized designs of heat source

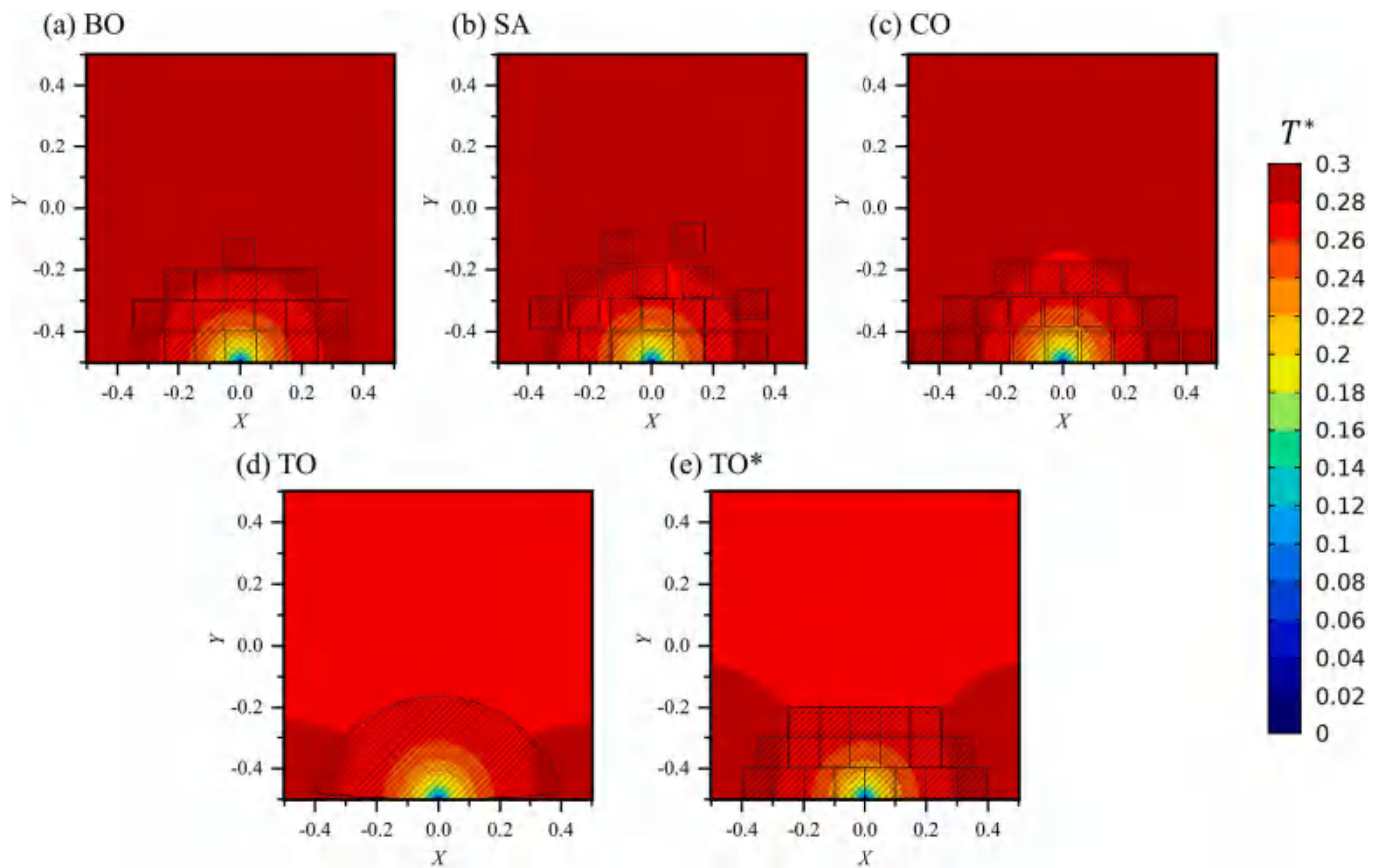


Fig. 8. Designs and temperature fields obtained by different optimization methods at  $\phi = 0.2$

**Table 1**  
Comparison of performance for different optimization methods at  $\phi = 0.2$ . The bold number denotes the best performance under the same metric.

Metrics	BO	SA	CO	TO	TO*
$T_{avg}^* (\times 10^{-1})$	2.677	2.667	2.705	<b>2.633</b>	2.646
$T_{max}^* (\times 10^{-1})$	2.848	2.851	2.967	<b>2.820</b>	2.847
$\sigma_T^* (\times 10^{-2})$	1.265	1.350	1.367	<b>1.251</b>	1.258
$D_p (\times 10^{-6} m^4)$	1.306	1.552	1.656	<b>1.295</b>	1.299

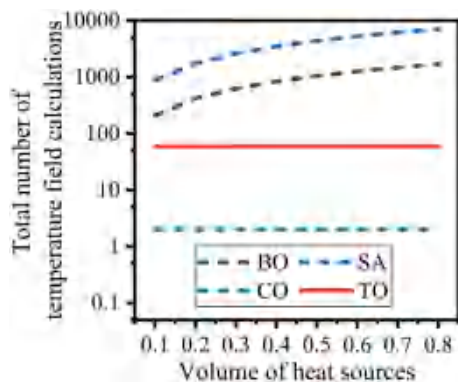


Fig. 9. The total number of temperature field calculations for different optimization methods varying with volume of heat sources.

distribution. The influence of heat source volume ( $\phi$ ) is investigated by the current TO method. The topology-optimized designs and temperature fields varying with  $\phi$  are shown in Fig. 10. With  $\phi$  increasing, the

heat source distribution expands around the side of the heat sink. However, due to the limitation of the whole system, the profile of the heat source distribution and the isotherms are no longer semicircle. In the three cases of  $\phi = 0.4, 0.6, 0.8$ , the computational costs are roughly the same due to the consistency of mesh number and other parameters, proving that  $\phi$  does not affect the efficiency of TO.

Except for  $\phi$ , the width of the heat sink is another important factor in engineering. TOs for  $\delta^* = 0.1, 0.4, 0.7$  with the same heat source volume ( $\phi = 0.1$ ) are conducted, and the results are shown in Fig. 11. Owing to the change in boundary conditions, the penalty factor for  $\delta^* = 0.4$  and  $\delta^* = 0.7$  is set to  $p = 0.4$ , and the upper limit of the iteration number is adjusted to 100 to obtain better optimized results. With the increase in  $\delta^*$ , the optimized design tends to be semielliptical from semicircular, while the isotherms are similar to the profile of the heat source distribution. For a wider heat sink, the optimized designs are still around the heat sink so that the heat source is as close as possible to the heat sink; thus, the topology-optimized heat source is wider in the  $x$  direction.

Since the wider heat sink cannot be regarded as a point, the definition of  $D_p$  with respect to the heat sink midpoint in Section 3.1 is no longer applicable. An equivalent distance function for the wide heat sink is defined. Taking the case of  $\delta^* = 0.4$  as an example, the streamlines of heat flux are plotted in Fig. 12(a), in which the streamline direction and the arrow size represent the local heat flux direction and the magnitude of heat flux, respectively. There is high heat flux at both endpoints of the heat sink where heat flow gathers, while the heat flux in the middle of the heat sink is low with the direction approximately perpendicular to the heat sink. Meanwhile, the total heat flux on the heat sink segment is plotted in the interior figure of Fig. 12(a), which further confirms that the heat flux is concentrated at the two ends of the heat sink. Inspired by this, a new equivalent distance  $D_t$  is defined by partitioning. As shown in Fig. 12(b), according to the location of heat sink endpoints  $P, Q$ , the optimized heat source domain is divided into three parts  $S_1, S_2, S_3$ . The

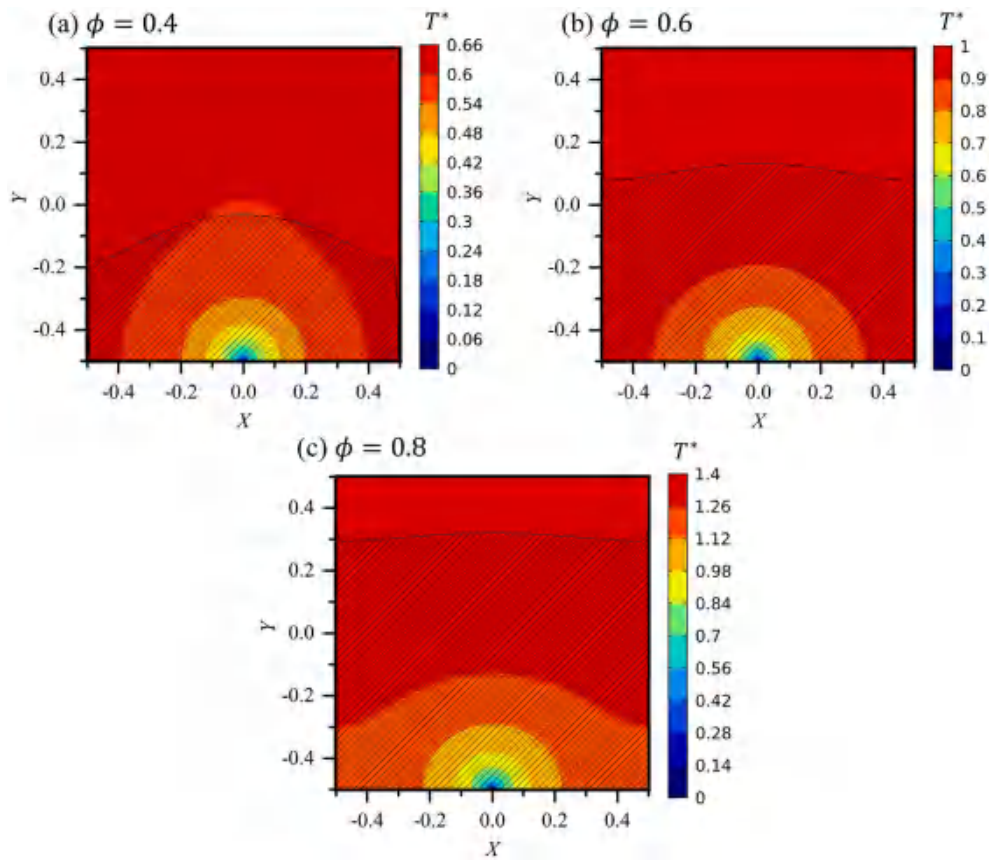


Fig. 10. Designs and temperature fields for different volumes of heat sources.

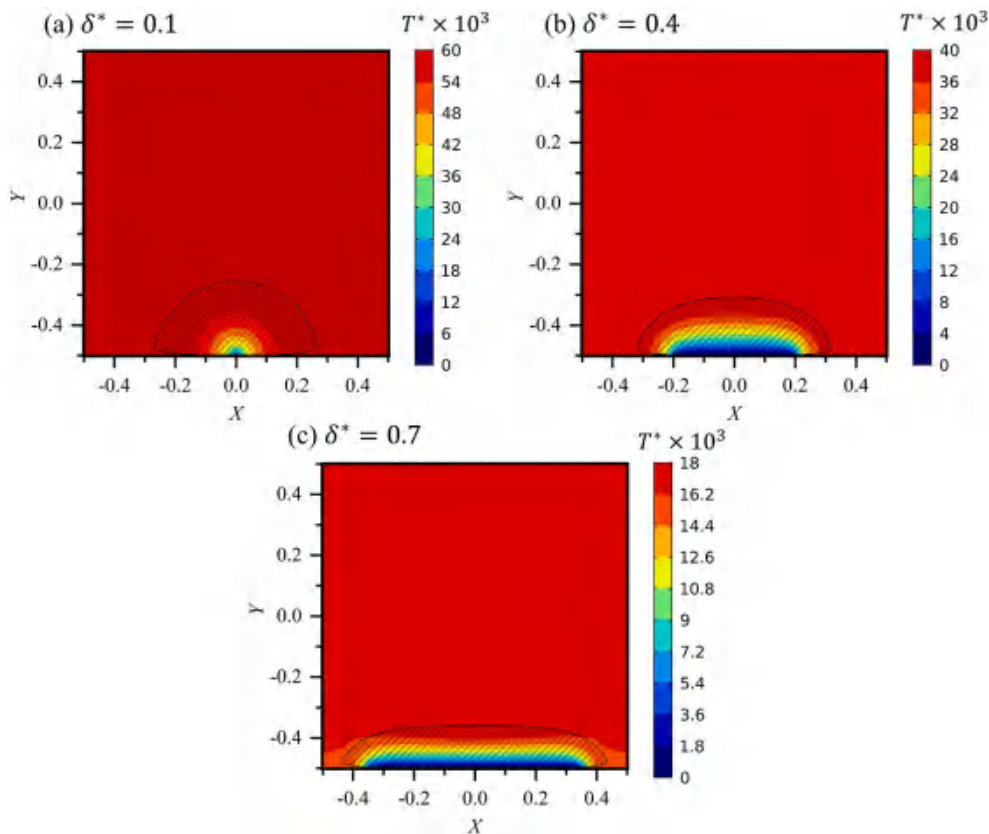


Fig. 11. Designs and temperature fields for different widths of the heat sink.

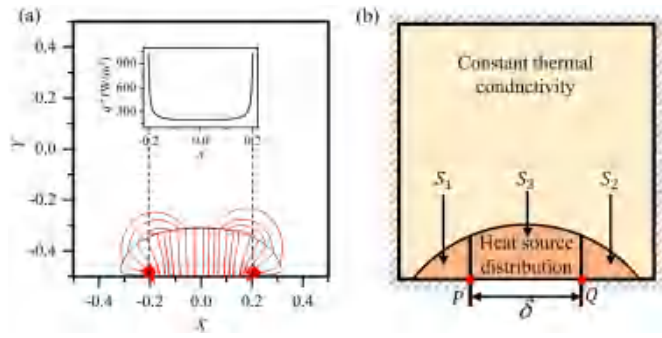


Fig. 12. Analyses of heat flux at  $\delta^* = 0.4$  and corresponding definition of equivalent distance function. (a) Heat flux field in the system and the total heat flux on the heat sink segment (inset); (b) the new definition of equivalent distance.

equivalent distance function  $D_P = \int_{S_1} r^2 dS_1$  of  $S_1$  with respect to point  $P$ ,  $D_Q = \int_{S_2} r^2 dS_2$  of  $S_2$  with respect to point  $Q$ , and  $D_{PQ} = \int_{S_3} y^2 dS_3$  with respect to line  $PQ$  are calculated, respectively; thus, it obtains  $D_t = D_P + D_Q + D_{PQ}$ . In Table 2,  $T_{avg}^*$  and  $D_t$  are evaluated for different optimized designs under different widths of the heat sink. The design of TO for specific heat source width has the lowest objective function value under the corresponding width, which verifies the effect of TO again.  $D_t$  shows the same variation trend as  $T_{avg}^*$ , and the design that has the lowest  $T_{avg}^*$  also obtains the lowest  $D_t$ . Therefore, it is reasonable to use  $D_t$  as a metric to determine the optimization performance under the condition of the wide heat sink.

#### 4. Conclusions

In this paper, topology optimization (TO) with the SIMP method and projection techniques is developed to solve the VP heat source distribution. Different from TO for the classical VP with filling high thermal conductivity materials, a penalty factor between 0 and 1 is adopted to interpolate the heat source intensity. Numerical tests show that  $p = 0.8$  is a reasonable value. An explicit mesh-independence check is conducted to determine reasonable values of the mesh size and the projection steepness.

Topology-optimized designs of different heat source volumes and heat sink widths are obtained. When the two parameters are small, the

Table 2

$T_{avg}^*$  and  $D_t$  for optimized designs evaluated under different widths of the heat sink. The bold number denotes the best performance for the same width (column).

	Evaluated at $\delta^*$					
	$T_{avg}^* (\times 10^{-2})$		$D_t (\times 10^{-7} m^4)$			
Designed at $\delta^*$	$\delta^* = 0.1$	$\delta^* = 0.4$	$\delta^* = 0.7$	$\delta^* = 0.1$	$\delta^* = 0.4$	$\delta^* = 0.7$
$\delta^* = 0.1$	5.00	1.47	1.03	<b>2.34</b>	1.50	1.49
$\delta^* = 0.4$	5.13	<b>1.19</b>	0.80	2.50	<b>1.09</b>	0.99
$\delta^* = 0.7$	6.03	1.59	<b>0.60</b>	3.95	1.18	<b>0.56</b>

profile of the optimized heat source is approximately semicircle, of which the center is located at the heat sink. The isotherms also look like semicircular arcs. As the heat source volume and the heat sink width increase, the topology-optimized designs are no longer semicircular but still around the heat sink. Theoretical analyses demonstrate that TO has basically obtained the optimal solution.

The function of the heat source domain is introduced for the evaluation of heat source distributions. The mechanism of different optimization methods to improve the heat transport is reducing the effective distance from the heat source to the heat sink, while the equivalent distance function characterizes this feature. Therefore, the variation trend of the equivalent distance function has good consistency with that of the temperature metrics.

The current TO has been proven to have better performance than BO, SA and CO in terms of reducing temperature and improving temperature uniformity. Moreover, the designs of TO are continuous, which can approximate the theoretical optimal solution better. In addition, the computational complexity of BO and SA is positively correlated with the number of heat sources, while the iteration number required for TO is basically independent. Therefore, TO can be conveniently used for the optimization of more heat sources. For the VP heat source distribution, TO indeed has advantages in performance, efficiency, and scalability.

#### Nomenclature

##### Variables

$c, d$	length and width of rectangular non-design area, m
$D_P$	equivalent distance function, $m^4$
$D_t$	developed equivalent distance function, $m^4$
$k$	constant thermal conductivity, $W/(m \cdot K)$
$n$	mesh number on square edge length
$p$	penalty factor
$\dot{Q}$	heat source intensity at any location in the whole system, $W/m^2$
$\dot{Q}_0$	constant heat source intensity, $W/m^2$
$S$	area of the whole system, $m^2$
$S_0$	area of the heat source domain, $m^2$
$T$	temperature, K
$T_0$	uniform temperature of the heat sink, K
$x, y$	horizontal and vertical coordinates of the system, m
$X, Y$	non-dimensional horizontal and vertical coordinates of the system
$\delta$	width of the heat sink, m
$\eta$	projection threshold parameter
$\rho$	design variable field
$\rho_p$	projected design variable
$\sigma$	projection steepness parameter
$\sigma_T^*$	non-dimensional standard deviation
$\phi$	volume constraint of heat sources

##### Superscripts

$i$	iteration number
*	non-dimensional value

##### Subscripts

avg	average value of the domain weighted by the heat source intensity
$j$	each mesh
max	maximum value

## Abbreviations

BO	bionic optimization
CO	convex optimization
DOF	degrees of freedom
IGBT	insulated-gate bipolar transistor
MCM	multi-chip module
SA	simulated annealing
SIMP	solid isotropic material with penalization
TO	topology optimization
VP	volume-to-point

## CRedit authorship contribution statement

**Zhi-Ke Liu:** Conceptualization, Methodology, Software, Validation, Formal analysis, Investigation, Data curation, Visualization, Writing – original draft. **Han-Ling Li:** Methodology, Software, Writing – review & editing. **Bing-Yang Cao:** Conceptualization, Supervision, Writing – review & editing, Project administration, Funding acquisition.

## Declaration of Competing Interest

The authors declare that they have no conflict of interest.

## Acknowledgements

This work was supported by National Natural Science Foundation of China (Grant Nos. U20A20301, 51825601).

## Appendix A. Supplementary data

Supplementary data to this article can be found online at <https://doi.org/10.1016/j.icheatmasstransfer.2022.106304>.

## References

- M. Chhowalla, D. Jena, H. Zhang, Two-dimensional semiconductors for transistors, *Nat. Rev. Mater.* 1 (2016) 16052.
- A. Asadi, F. Pourfatah, Effects of constructal theory on thermal management of a power electronic system, *Sci. Rep.* 10 (2020) 21436.
- A.L. Moore, L. Shi, Emerging challenges and materials for thermal management of electronics, *Mater. Today* 17 (2014) 163–174.
- M.M. Waldrop, The chips are down for Moore's law, *Nature* 530 (2016) 144–147.
- Y. Hua, H. Li, B. Cao, Thermal spreading resistance in ballistic-diffusive regime for GaN HEMTs, *IEEE Transact. Electron Dev.* 66 (2019) 3296–3301.
- L.T. Yeh, Review of heat transfer Technologies in Electronic Equipment, *J. Electron. Packag.* 117 (1995) 333–339.
- M. Pedram, S. Nazarian, Thermal modeling, analysis, and management in VLSI circuits: principles and methods, *Proc. IEEE* 94 (2006) 1487–1501.
- S.M. Sohel Murshed, C.A. Nieto De Castro, A critical review of traditional and emerging techniques and fluids for electronics cooling, *Renew. Sust. Energ. Rev.* 78 (2017) 821–833.
- Z. He, Y. Yan, Z. Zhang, Thermal management and temperature uniformity enhancement of electronic devices by micro heat sinks: a review, *Energy* 216 (2021), 119223.
- F. Tavakkoli, S. Ebrahimi, S. Wang, K. Vafai, Analysis of critical thermal issues in 3D integrated circuits, *Int. J. Heat Mass Transf.* 97 (2016) 337–352.
- J.L. Smoyer, P.M. Norris, Brief historical perspective in thermal management and the shift toward Management at the Nanoscale, *Heat Transfer Eng.* 40 (2019) 269–282.
- J. Fukai, M. Kanou, Y. Kodama, O. Miyatake, Thermal conductivity enhancement of energy storage media using carbon fibers, *Energy Convers. Manag.* 41 (2000) 1543–1556.
- P. Mańkowski, A. Dominiak, R. Domański, M.J. Kruszewski, A. Ciupiński, Thermal conductivity enhancement of copper–diamond composites by sintering with chromium additive, *J. Therm. Anal. Calorim.* 116 (2014) 881–885.
- A. Bejan, Constructal-theory network of conducting paths for cooling a heat generating volume, *Int. J. Heat Mass Transf.* 40 (1997) 799–816.
- X. Cheng, Z. Li, Z. Guo, Constructs of highly effective heat transport paths by bionic optimization, *Sci. China Series E: Technol. Sci.* 46 (2003) 296–302.
- J. Dirker, J.P. Meyer, Topology optimization for an internal heat-conduction cooling scheme in a square domain for high heat flux applications, *J. Heat Transfer -Transact. ASME* 135 (2013), 111010.
- A. Gersborg-Hansen, M.P. Bendsoe, O. Sigmund, Topology optimization of heat conduction problems using the finite volume method, *Struct. Multidiscip. Optim.* 31 (2006) 251–259.
- T. Gao, W.H. Zhang, J.H. Zhu, Y.J. Xu, D.H. Bassir, Topology optimization of heat conduction problem involving design-dependent heat load effect, *Finite Elem. Anal. Des.* 44 (2008) 805–813.
- X. Xu, X. Liang, J. Ren, Optimization of heat conduction using combinatorial optimization algorithms, *Int. J. Heat Mass Transf.* 50 (2007) 1675–1682.
- W. Du, P. Wang, L. Song, L. Cheng, Optimization of volume to point conduction problem based on a novel thermal conductivity discretization algorithm, *Chin. J. Chem. Eng.* 23 (2015) 1161–1168.
- B. Li, J. Hong, L. Ge, C. Xuan, Designing biologically inspired heat conduction paths for 'volume-to-point' problems, *Mater. Des.* 130 (2017) 317–326.
- B. Li, J. Hong, X. Tian, Generating optimal topologies for heat conduction by heat flow paths identification, *Int. Communicat. Heat Mass Transfer* 75 (2016) 177–182.
- A. Iradukunda, A. Vargas, D. Huitink, D. Lohan, Transient thermal performance using phase change material integrated topology optimized heat sinks, *Appl. Therm. Eng.* 179 (2020), 115723.
- H. Li, D. Lan, X. Zhang, B. Cao, Investigation of the parameter-dependence of topology-optimized heat sinks in natural convection, *Heat Transfer Eng.* 43 (2022) 922–936.
- A. Fawaz, Y. Hua, S. Le Corre, Y. Fan, L. Luo, Topology optimization of heat exchangers: a review, *Energy* 252 (2022), 124053.
- T. Dbouk, A review about the engineering design of optimal heat transfer systems using topology optimization, *Appl. Therm. Eng.* 112 (2017) 841–854.
- L. Xu, L. Pu, S. Zhang, L. Nian, Y. Li, Structure optimization design of ground heat exchanger by topology method to mitigate the geothermal imbalance, *Appl. Therm. Eng.* 170 (2020), 115023.
- Y. Zhang, S. Liu, Design of conducting paths based on topology optimization, *Heat Mass Transf.* 44 (2008) 1217–1227.
- V. Subramaniam, T. Dbouk, J.L. Harion, Topology optimization of conductive heat transfer devices: an experimental investigation, *Appl. Therm. Eng.* 131 (2018) 390–411.
- H. Li, B. Cao, Topology optimization of the volume-to-point heat conduction problem at micro- and nano-scale, *Acta Phys. Sin.* 68 (2019), 200201.
- P. Yang, X. Qin, A hybrid optimization approach for chip placement of multi-chip module packaging, *Microelectron. J.* 40 (2009) 1235–1243.
- T. Suwa, H. Hadim, Multidisciplinary heat generating logic block placement optimization using genetic algorithm, *Microelectron. J.* 39 (2008) 1200–1208.
- H. Delaram, A. Dastfan, M. Norouzi, Optimal thermal placement and loss estimation for power electronic modules, *IEEE Trans. Compon. Packag. Manuf. Technol.* 8 (2018) 236–243.
- R.R. Madadi, C. Balaji, Optimization of the location of multiple discrete heat sources in a ventilated cavity using artificial neural networks and micro genetic algorithm, *Int. J. Heat Mass Transf.* 51 (2008) 2299–2312.
- S. Soleimani, D.D. Ganji, M. Gorji, H. Baramia, E. Ghasemi, Optimal location of a pair heat source-sink in an enclosed square cavity with natural convection through PSO algorithm, *Int. Communicat. Heat Mass Transfer* 38 (2011) 652–658.
- K. Chen, S. Wang, M. Song, Optimization of heat source distribution for two-dimensional heat conduction using bionic method, *Int. J. Heat Mass Transf.* 93 (2016) 108–117.
- K. Chen, S. Wang, M. Song, Temperature-gradient-aware bionic optimization method for heat source distribution in heat conduction, *Int. J. Heat Mass Transf.* 100 (2016) 737–746.
- K. Chen, J. Xing, S. Wang, M. Song, Heat source layout optimization in two-dimensional heat conduction using simulated annealing method, *Int. J. Heat Mass Transf.* 108 (2017) 210–219.
- Y. Aslan, J. Puskely, A. Yarovoy, Heat source layout optimization for two-dimensional heat conduction using iterative reweighted L1-norm convex minimization, *Int. J. Heat Mass Transf.* 122 (2018) 432–441.
- Q. Chen, H. Zhu, N. Pan, Z. Guo, An alternative criterion in heat transfer optimization, *Proceed. Royal Soc. A: Math. Phys. Eng. Sci.* 467 (2011) 1012–1028.
- Q. Chen, X. Liang, Z. Guo, Entransy theory for the optimization of heat transfer - a review and update, *Int. J. Heat Mass Transf.* 63 (2013) 65–81.
- F. Li, J. Ning, S.Y. Liang, Analytical modeling of the temperature using uniform moving heat source in planar induction heating process, *Appl. Sci.* 9 (2019) 1445.
- J. Ning, D.E. Sievers, H. Garmestani, S.Y. Liang, Analytical modeling of transient temperature in powder feed metal additive manufacturing during heating and cooling stages, *Appl. Phys. A* 125 (2019) 496.
- J. Ning, S.Y. Liang, A comparative study of analytical thermal models to predict the orthogonal cutting temperature of AISI 1045 steel, *Int. J. Adv. Manuf. Technol.* 102 (2019) 3109–3119.
- M.P. Bendsoe, O. Sigmund, Optimization of Structural Topology, Shape, and Material, Springer, Berlin, Germany, 1995.
- M.P. Bendsoe, O. Sigmund, Material interpolation schemes in topology optimization, *Arch. Appl. Mech.* 69 (1999) 635–654.
- J.D. Deaton, R.V. Grandhi, A survey of structural and multidisciplinary continuum topology optimization: post 2000, *Struct. Multidiscip. Optim.* 49 (2014) 1–38.
- O. Sigmund, A 99 line topology optimization code written in Matlab, *Struct. Multidiscip. Optim.* 21 (2001) 120–127.
- A. Rietz, U. Linköpings, F.K.O.P. Institutionen, H. Tekniska, Sufficiency of a finite exponent in SIMP (power law) methods, *Struct. Multidiscip. Optim.* 21 (2001) 159–163.
- G.I.N. Rozvany, A critical review of established methods of structural topology optimization, *Struct. Multidiscip. Optim.* 37 (2009) 217–237.

- [51] O. Sigmund, Morphology-based black and white filters for topology optimization, *Struct. Multidiscip. Optim.* 33 (2007) 401–424.
- [52] F. Wang, B.S. Lazarov, O. Sigmund, On projection methods, convergence and robust formulations in topology optimization, *Struct. Multidiscip. Optim.* 43 (2011) 767–784.
- [53] M.P. Bendsoe, O. Sigmund, *Topology Optimization: Theory, Methods, and Applications*, Springer Science & Business Media, Berlin, 2004.
- [54] K. Svanberg, The method of moving asymptotes—a new method for structural optimization, *Int. J. Numer. Methods Eng.* 24 (1987) 359–373.